Grain refinement and hardness saturation in pure Nickel subjected to a sequence of ECAP and HPT

M. Cabibbo

A detailed investigation was carried out to describe the microstructure grain refinement process and hardness evolution of pure nickel processed using a combination of two severe plastic deformation (SPD) techniques: equal-channel angular pressing (ECAP) and high-pressure torsion (HPT). Two different shear deformation modes were used and compared: a co-operating shear deformation in which the same sense of sample rotation between ECAP and HPT was maintained; a reversing shear deformation in which the sense of rotation was inverted between ECAP and HPT. ECAP was conducted using the route B_C in which the sample was rotated counter clockwise by 90° between passes for up to 4 passes. Hardness was measured using nanoindentation techniques. It was found that the combination of ECAP + HPT allowed an effective grain refinement and hardening of nickel. Microstructure cell and grain refinement to sub-micrometer levels, and a significant metal hardening was achieved already at low ECAP + HPT strain regimes, thus demonstrating the beneficial synergic effect of the two plastic shear deformation techniques. Saturation limits in terms of cell size reduction (~ 280 nm) and of hardness rise with cumulative straining ($\varepsilon_{true}^{ECAP+HPT} > 7.5$) were reached at ECAP-$B_C$/4 + HPT for P = 6 GPa and N = 1 counter clockwise revolution, and it was anticipated to P = 3 GPa as the number of revolutions doubled.

KEYWORDS: ECAP - HPT - PURE NICKEL - TEM - NANOINDENTATION - GRAIN REFINEMENT

INTRODUCTION

There is much current interest in producing metals with very small grain sizes. This interest is due because a reduction in grain size leads to significant material strength and toughness improvement at room temperature. Nickel has a stacking fault energy (SFE) intermediate between metals with high SFE, namely aluminium, and those with relatively low SFE, of which copper is a good example. Moreover, nickel is able to produce smaller grain sizes than pure Al and has a more homogeneous structure than pure Cu [1,2].

Most of the procedures currently in use for producing ultra-fine grained bulk materials involve severe plastic deformation (SPD) techniques [3-7]. There are two principal methods for subjecting a metallic material to severe plastic deformation: equal-channel angular pressing (ECAP) and high-pressure torsion (HPT). The principle of processing through ECAP was first proposed in the former Soviet Union more than 30 years ago [8]. Subsequently, it was recognized that this processing technique leads to very substantial grain refinement in the metallic material [9,10]. Processing by HPT has two advantages of producing exceptionally small grain sizes, often in the nanometer range (some 100 nm, and below). Nevertheless, HPT has the disadvantage that the specimen sizes are generally fairly small, with maximum disk diameters and thicknesses typically of ~20 and ~1 mm, respectively [11]. The microstructure evolution of pure nickel, processed through ECAP and HPT has been reported to induce more effective grain refinement after HPT than after ECAP [1,2]. Both the methods produce a large fraction of high-angle boundaries.

The average grain size reduction during ECAP depends on several parameters including the processing route and the number of passes. In ECAP, the material, in the form of a rod orbar, is pressed repetitively through a channel bent through an abrupt angle, while in HPT, the sample, in the form of a thin disk, is subjected to high pressure and concurrent torsion straining. Several experimental results have demonstrated that when a metallic material is processed by HPT, grain refinement is more effective than when it is subjected to ECAP [12-14].

Since HPT processing produces a significantly smaller grain size than ECAP, it is interesting to examine the microstructure

Marcello Cabibbo
Department of Industrial Engineering and Mathematics (DIISM), Università Politecnica delle Marche, 60131 Ancona, Italy

modifications produced by combining ECAP followed by HPT. This type of experiment was first conducted by Stolyarov et al. [15] using commercial purity Ti, and they reported that processing by HPT after ECAP produces additional refinement in grain size and a consequent increase in hardness. More recently, other experiments on Ni [13,16] and on a Cu-0.1% Zr alloy [17] have also confirmed the occurrence ofa significant reduction in grain size after a combination of ECAP and HPT.

Recently, Popov et al. [18-20] reported a grain size reduction of commercially pure Nb after a combination of ECAP and HPT, which turned out to be the same as by processing the material only by HPT. It was claimed that there is a saturation limit which did not allow either additional refining of the grains or additional hardening. This actually suggests that there is a limiting value on the level of grain refinement that may be achieved under any specific SPD technique, and the precise significance of this level of saturation has been the subject of extensive speculation [23,24]. There are numerous uncertainties associated with the production of saturation grain sizes in HPT processing including, for example, whether this minimum grain size is affected by any preliminary processing that may be conducted prior to HPT.

Present work focused on the microstructure cell and grain refinement potentials and on the evolution of hardness with cumulative straining generated by the combined use of ECAP followed by HPT. Two different shear deformation paths were followed during HPT (modes). In one mode the same shear deformation sense between HPT and the previous ECAP was followed. In a second mode the thin HPT disk was made to follow a shear deformation sense opposite respect to the deformation sense followed by the section of the cylindrical billet during ECAP. The present study shows that a saturation limit is achieved in commercially pure Ni subjected to ECAP + HPT. This saturation was obtained in terms of both microstructure refinement and nano-hardness. In this work, the hardness was measured by nanoindentation, thus reaching a measurement sensitivity of $<$ 1 μm (the nanoindentation print and penetration depth being typically of around 0.8-to-1.1 μm). The combination of ECAP + HPT was able to refine the pure nickel cell structure down to less than ~300 nm, and it also led to a hardness increase by up to 5 times compared to the initial undeformed nickel hardness.

EXPERIMENTAL PROCEDURES AND METHOD

The commercially pure nickel used in this work has a chemical composition as shown in the Table 1. In order to homogenize the initial grained structure, samples were annealed for 6 h at 973 K prior to severe plastic deformation (SPD), i.e., ECAP + HPT. This initial heat treatment gave a relaxed microstructure with an initial grain size of 90 ± 2 μm and an initial hardness of 0.8 ± 0.1 GPa.

Al	C	Si	Fe	Mg	Mn	Co	Ti	P	Cu	Cr	S	Ni
0.004	0.003	0.003	0.003	0.003	0.002	0.002	0.002	0.002	0.001	0.0003	0.0001	Bal.

Tab. 1 - Chemical composition of the commercially pure nickel used in this study (wt.%).
Composizione chimica del Nichel commercialmente puro, utilizzato nel presente studio (% in peso).

Ni (99.975 wt.% of purity) was severely deformed by ECAP at room temperature using the route B_C, i.e., by pressing the specimen through a die and rotating it by 90° (counter clockwise) about the long axis in the same direction after each pass, N, [21]. ECAP billets were machined so as to have diameters of 9.8 mm and lengths of 50 mm. Samples were pressed into the ECAP die using a dedicated hydraulic press, with forces ranging between 40-80 kN and a pressing speed of 40 mm/min.

The ECAP die consisted of two blocks of SK3 tool steel (Fe-1.1%C) which were bolted together to give an L-shaped channel with a circular cross-section of 10 mm in diameter consisting of two linear parts intersecting at an angle $\Phi = 90°$ with a curvature extending over an angle $\Psi = 20°$. Using this die configuration, the shear strain imposed at each pass, $\varepsilon_{true}^{ECAP}$, is given by Eq. (1) [22]:

$$\varepsilon_{true}^{ECAP} = \frac{N}{\sqrt{3}}\left[2cot\left(\frac{\Phi}{2}+\frac{\Psi}{2}\right)+\Psi cosec\left(\frac{\Phi}{2}+\frac{\Psi}{2}\right)\right] \quad (1)$$

With this die configuration, and according to Eq. (1), a true strain of $\varepsilon_{true}^{ECAP} = 1.08$ was imposed on the specimens at each pass. The material was subjected to a total of 4 passes, giving a maximum equivalent strain $\varepsilon_{true}^{ECAP} = 4.32$.

After processing, the ECAP billets were cut perpendicular to their longitudinal axes to provide a series of disks with thicknesses of 1.5 mm which were mechanically polished to flatness to a typical thickness of 1.20 ± 0.05 mm. The polished disks (9.8 in diameter and 1.20 thick) were processed by HPT at room temperature. HPT was exerted by a home-made servo-hydraulic computer-assisted torsion machine. HPT samples were deformed between an upper and a lower anvil which were pressed together, the upper anvil being the one which rotates. In the present investigation, the applied pressures were 1, 3, 6, and 9 GPa, for 1 and 2 complete revolutions. Samples weredeformed with a rotation speed of 2 rpm, corresponding to a strain rate $\dot{\varepsilon} = 0.08\ .\ s^{-1}$. HPT processing wasperformed under so-called unconstrained conditions so that thedeformed material was free to flow outwards between the anvils during the processing operation. Fig. 1 shows the steady disk radial increment with HPT pressure, P, and number of revolutions, N.

It appears that the maximum disk radial spreading was up to 12 and 14 mm, for P = 9 GPa, N = 1, and N = 2 revolutions, respectively. This marginally reduced the sample thicknesses from ~1 down to ~0.6 mm after HPT deformation (from P = 1 GPa, N = 1, to P = 9 GPa, N = 2).

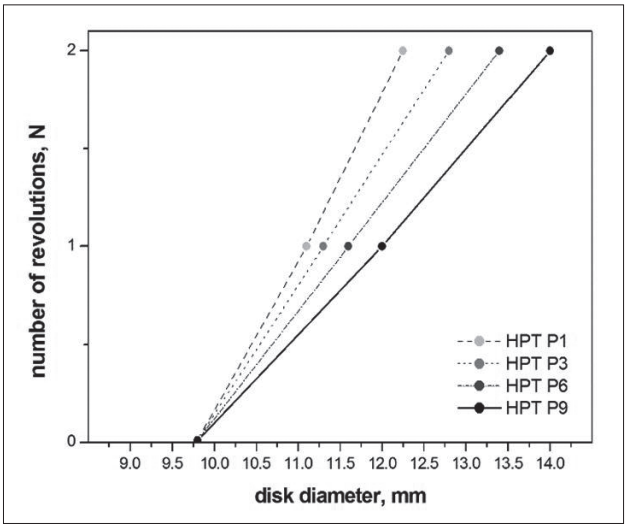

Fig. 1 - HPT disk radial increment with shear deformation (P = 1, 3, 6, 9 GPa, and N = 1 and 2 revolutions).
Incremento radiale imposto dalla deformazione HPT (P = 1, 3, 6, 9 GPa, e N = 1, 2 rotazioni complete).

The principles of HPT processing can be schematically described as follows. Surface frictional forces deform the disk byshear so that deformation proceeds under a quasi-hydrostatic pressure. The strain, dγ, imposed in HPT for an infinitely small rotation, dθ, and displacement, dl as dl = rdθ, where r isthe radius of the disk), is given by: dγ = rdθ/t, where t is the disk thickness. Assuming the thickness of the disk as independent of the rotation angle, θ, formal integration can be used.
Thus, the equivalent strain $\varepsilon = \gamma/\sqrt{3}$, and the true logarithmic strain, ε_{true}^{HPT}, is Eq. (2a) [23]:

$$\varepsilon_{true}{}^{HPT} = \ln(1+\varepsilon) = \ln\left(1+\frac{\theta r}{t\sqrt{3}}\right) \approx \ln\left(\frac{\theta r}{t\sqrt{3}}\right) \quad (2a)$$

An alternative relationship, which actually incorporates the disk thickness reduction with the applied pressure, P, is given after [23] by Eq. (2b):

$$\varepsilon_{true}{}^{HPT} = \ln\left(1+\left(\frac{\theta r}{t}\right)^2\right)^{1/2} + \ln\left(\frac{t_0}{t}\right) \quad (2b)$$

where t_0, and t are the initial and final disk thicknesses, respectively. Since (θr/t)»1, Eq. (1b) can be rewritten as Eq. (2c):

$$\varepsilon_{true}{}^{HPT} = \ln\left(1+\left(\frac{\theta r}{t}\right)\right) + \ln\left(\frac{t_0}{t}\right) \quad (2c)$$

In this respect, it was reported [23,24] that the difference between Eq. (2a) and Eq. (2c) is less than 20%.
Two rotation directions were taken into consideration. One in accordance with the sense of rotation of the previous ECAP-B_C which was counter clockwise and the other in the opposite sense, that is clockwise. The counter clockwise ECAP-B_C + HPT deformation mode was named as co-operating-shear strain (CSS) deformation mode; the counter clockwise ECAP-B_C + clockwise (reverse) HPT mode was named as reversing-shear strain (RSS) deformation mode.
Nanoindentation hardness measurements were performed on the circular sections of the samples after ECAP + HPT (i.e., normal plane in ECAP, Z, and shear plane normal direction in HPT, SPN). To this purpose, disk surface was smoothly mechanical polished using 0.25 μm diamond paste. Hardness measurements were performed at N = 1, and 2 revolutions for all the pressure levels (i.e., P = 1, 3, 6, 9 GPa). These measurements were taken along two mutually perpendicular diameters at positions 300 μm apart. The average microhardness was determined from a square grid, 200 μm of edge, of 2x2 individual measurements clustered around the selected position so as to have the reference position along the disk diameter right in the center of the square grid. With this measurement methodology, each plotted point results from an average value of 4 individual measurements clustered around positions spaced 300 μm one to the follower, and the square grid of 200 μm makes the individual measurements to be spaced 100 μm. The plots of the nanoindentation hardness (GPa unit), as a function of the position on the disk surface, were thus realized averaging the two sets of measurements taken along the two mutually perpendicular diameters at a homologous position with respect to the center of the disk. Nanoindentation measurements were carried out using a UBI-1® Hysitron™ Triboscan nanoindenter, equipped with a triangular Berkovich tip. Tip calibration was carried out using a standard procedure [25-27]. The maximum load was fixed at 10 mN. A trapezoidal load function (30 s load to the maximum load value, maintenance for 10 s, and unloading in 30 s) was used. The nanoindentation measurements were analyzed using the Oliver and Pharr method

[25,26,28]. The unloading curve is fitted with a power-law relationship, Eq. (3a):

$$L = B(h-h_f)^m \quad (3a)$$

where L is the tip load, h the displacement, h_f is the displacement after unloading, B and m are fitting parameters. The contact depth, h_c, can be estimated from the load-displacement data as (Eq. 3b):

$$h_c = h_{max} - \varepsilon(L_{max}/S) \quad (3b)$$

where h_{max} is the maximum indenter penetration depth at peak load, L_{max}, ε is a tip dependent constant, and S is the material stiffness. For the Berkovich tip, $\varepsilon = 0.75$ [25,26,28]. Calibration was carried out on fused quartz ($E_r = 72$ GPa) according to the specifications and recommendation resulting from a round robin experiment recently published by M. Cabibbo et al. [26,27].

The use of nanoindentation, for the determination of the hardness across the ECAP and HPT samples, gives a data accuracy of 2% and a lateral sensitivity of ~ 1 μm.

Microstructure inspections and quantitative analyses were performed by the transmission electron microscopy (TEM) technique. Thin foils were sliced parallel to the circle section of the cylindrical bars (thus allowing the inspection of the planes normal to the ECAP direction, plane Z) and prepared by mechanical polishing to surface flatness, dimpling, and ion-milling by a Gatan™ PIPS®. A Philips™ CM20 TEM operated at 200 kV, and equipped with a double tilt specimen holder, was used. All microstructural observations were made on the disk (shear) plane at the mid-radius location. Grain and cell sizes were quantified by stereological methods. Thus, boundary spacing was calculated using the linear intercept method. The average boundary intercept distance was calculated based on the average orthogonal boundary intercept spacings, L_X and L_Y, where the suffixes X and Y stand for the two mutually orthogonal directions. Therefore, the average boundary spacing $L_{XY} = 1/N_{LXY}$, where $N_{LXY} = (1/L_X + 1/L_Y)/2$ is the number of boundary intercepts per unit of test line length along X and Y [29].

RESULTS

The homogenized 99.975 wt.% purity Ni (whose microstructure is shown in Fig. 2) was first subjected to 1-to-4 ECAP via route B_C. Cell spacing distributions were determined by TEM inspections and the linear intercept method (EN-112), and results are shown in Fig. 3. It appeared that a reduction of 1/4 of the initial mean grain size (i.e., from 80 to 22 μm) was achieved after the first ECAP pass, while a further significant reduction down to 2.9 μm, and thus almost to one-order of magnitude, was obtained after ECAP-B_C/4 passes. The spacing distribution was fairly spread at ECAP/1, spanning from 6 to 44 μm, and it shrunk significantly at ECAP-B_C/4, spanning form 0.5 to 6 μm. Accordingly, the distribution peak increased with the cumulative shear deformation.

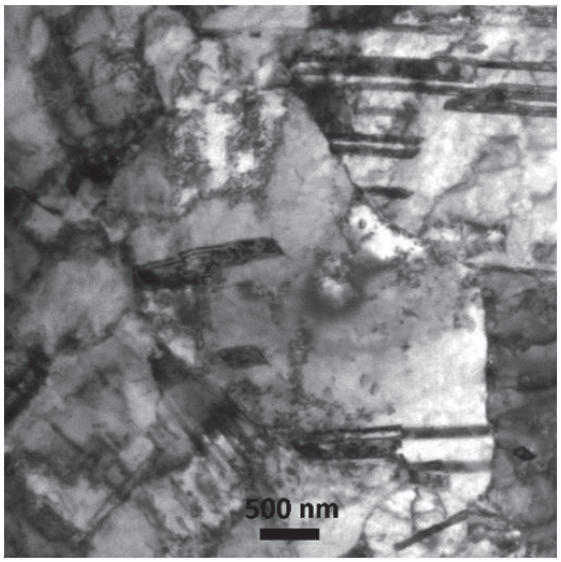

Fig. 2 - Microstructure of homogenized pure nickel (annealing at 973 K / 6 h).
Microstruttura del Nichel, commercialmente puro, nello stato omogeneizzato inziale (973 K / 6 h).

The Ni microstructure evolution with cumulative strain when subjected to HPT after ECAP is shown in Fig. 4, where representative TEM images at maximum pressure, P = 9 GPa, after N = 2 revolutions are reported. After ECAP/1 + HPT, the microstructure appeared to be characterized by a considerable tangle dislocation with traces of twinning (Fig. 4a). More specifically, the microstructure after ECAP/1 + HPT (P = 9 GPa, N = 2 revolutions) appeared similar to the one obtained after ECAP-B_C/4 + HPT (P = 9 GPa, N = 2 revolutions) processed by the reversing-shear strain (RSS) deformation mode (according to the acronyms given in the Experimental procedures and method section).

After ECAP-B_C/4 + HPT (P = 9 GPa, N = 2 revolutions), processed by the co-operating-shear strain (CSS) deformation mode,

the microstructure showed sharper grain boundaries with a significant lower fraction of tangled dislocations with respect to the RSS microstructure (Fig. 4b,c). As a matter of fact, the RSS microstructure differentiate compared to what was obtained by CSS since a much less refined grained structure was achieved by RSS than by the CSS deformation mode.

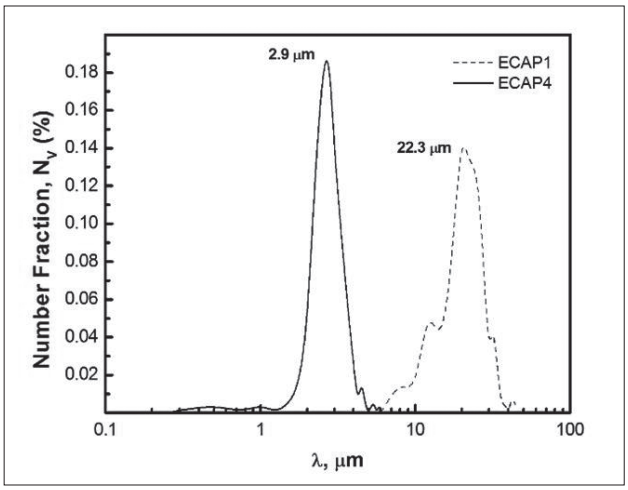

Fig. 3 - Cell spacing distribution of ECAP/1, and ECAP-B_C/4, taken along the plane Z.
The value of the mean cell size is reported in the graph next to the corresponding distribution.
Distribuzione spaziale delle celle (sottograni) dopo ECAP/1, e ECAP-B_C/4, lungo il piano Z.
Il valore medio della spaziatura delle celle è riportato in corrispondenza delle relative curve di distribuzione.

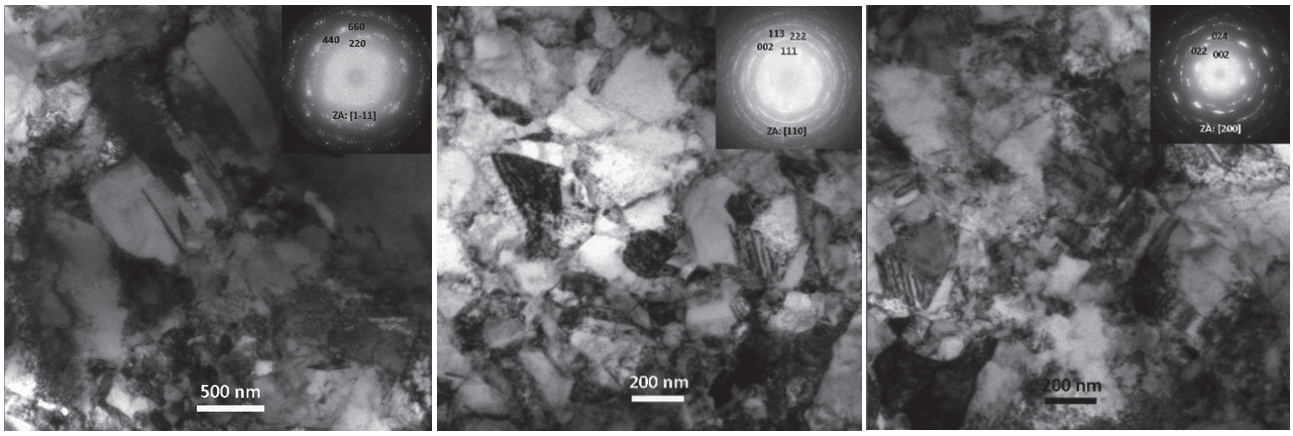

a) b) c)

Fig. 4 - Representative microstructure evolution with maximum shear deformation for ECAP/1 + HPT (P = 9 GPa, N = 2 revolutions), a); ECAP-B_C/4 + CSS HPT (P = 9 GPa, N = 2 revolutions), b); and ECAP-B_C/4 + RSS HPT (P = 9 GPa, N = 2 revolutions), c).
Microstruttura rappresentativa del Nichel commercialmente puro, dopo ECAP/1 + HPT (P = 9 GPa, N = 2), a);
ECAP-B_C/4 + CSS HPT (P = 9 GPa, N = 2), b); ECAP-B_C/4 + RSS HPT (P = 9 GPa, N = 2), c).

The cell spacing evolution with HPT pressure and revolutions after the first ECAP shear deformation is reported in Fig. 5. The grain spacing distribution clearly showed an evident size reduction with pressure characterized by similar size reduction rate between 1 and 2 revolutions. In general, the distribution peaks slightly increased with the HPT pressure, as well as a slight shrink of the distribution width, with the HPT shear deformation occurred. Cell spacing reduced, from a mean value of 22.3 μm of ECAP-1 down to 1.1 and 0.5 μm, at HPT P = 9 GPa, N = 1, and N = 2, respectively. Thence, the applied pressure under HPT induced a large amount of grain size refinement, from ~10 μm, at P = 1 GPa, to 1.1 μm, at P = 9 GPa, for N = 1 revolution, and from ~7.5 μm, at P = 1 GPa, to 0.5 μm, at P = 9 GPa, for N = 2 revolutions. Given fixed HPT pressure, the grain size typically halved as the number of revolutions duplicated (i.e., from 1 to 2), with the only exception of what has incidentally been reported for P = 1.

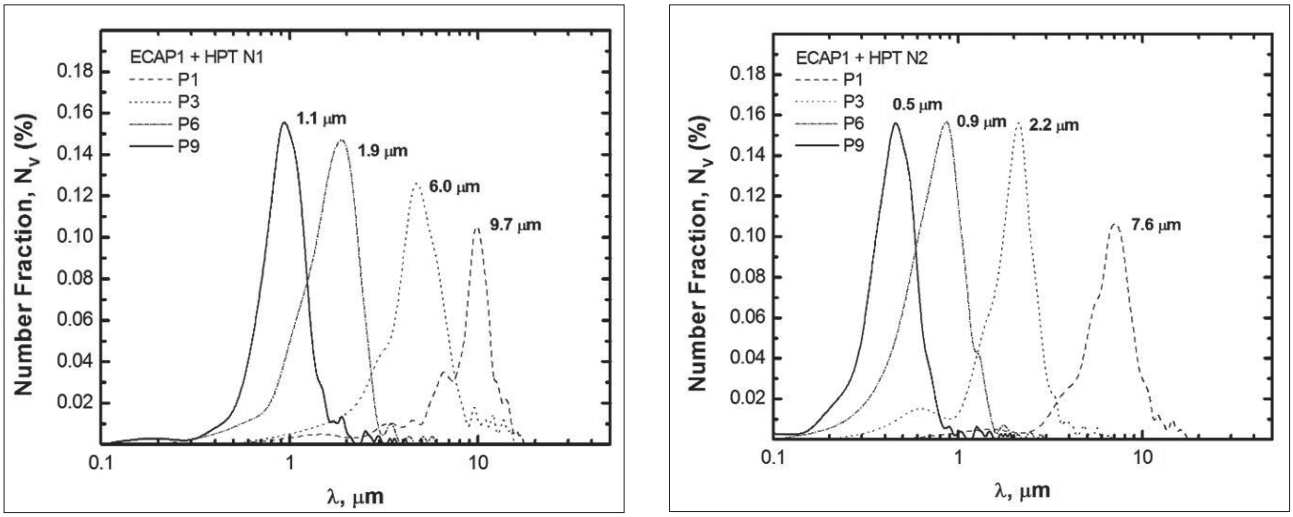

a) b)

Fig. 5 - Cell spacing evolution with ECAP/1 + HPT (P = 1-to-9 GPa), N = 1 revolution, a); N = 2 revolutions, b). Mean grain size is reported in the graph next to the corresponding distribution.
Evoluzione della spaziatura delle celle dopo ECAP/1 + HPT (P = 1-9 GPa), N = 1, a); N = 2, b). I valori medi sono riportati in corrispondenza delle curve di distribuzione.

The grain spacing evolution is far less linear and, to some extent, more complicated in the case of a full cycle of shear ECAP deformation using route B_C. Here, another interesting aspect is constituted by the two different rotation senses imposed on HPT, compared to the previous counter clockwise rotation induced by ECAP route B_C.
After ECAP-B_C/4 + HPT in both cases of concurrent and opposite rotation direction compared to the ECAP-B_C one (CSS and RSS modes), the cell spacing distribution appeared to shrink and to increment the size peak as the HPT shear cumulate, by increasing pressure, P, as well as increasing the number of revolutions, from N = 1 to 2 (Fig. 6).
However, an interesting evolutionary aspect differentiated the distribution of the CSS HPT mode compared to the RSS one. In the latter case, the cell spacing distribution evolved steadily to size reduction down to 0.5 μm (P = 9 GPa, N = 1 revolution) and 0.3 μm (P = 9 GPa, N = 2 revolutions), as seen in Fig. 6c,d. On the contrary, by CSS HPT mode, a saturation limit of the size appeared, and this was reached for P = 6 GPa, at N = 1 revolution and anticipated to P = 3 GPa, at N = 2 revolutions, as shown in Fig. 6a,b. The saturation limit value was ~0.3 μm. It is believed that a saturation limit of ~0.3 μm grain lateral spacing is likely to occur also by using the RSS HPT mode for larger deformation regimes, i.e., higher HPT pressures and number of revolutions. Finally, it is worth noting that the size reduction rate between N = 1 and N = 2 revolutions, at fixed HPT pressures, is lower when the material is previously subjected to four ECAP-B_C passes, compared to a single ECAP pass.

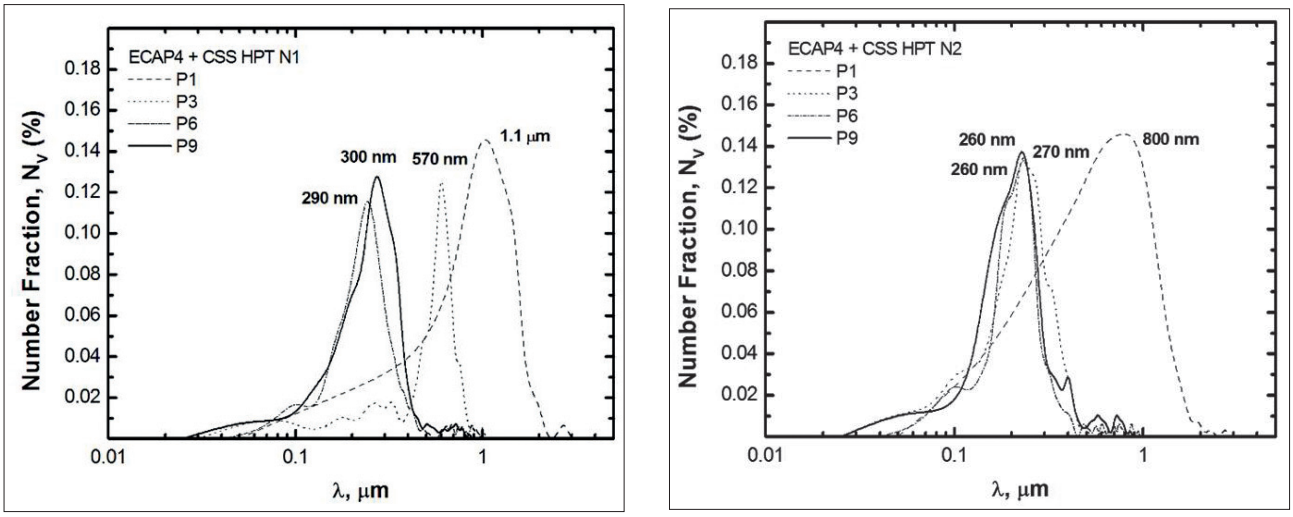

a) b)

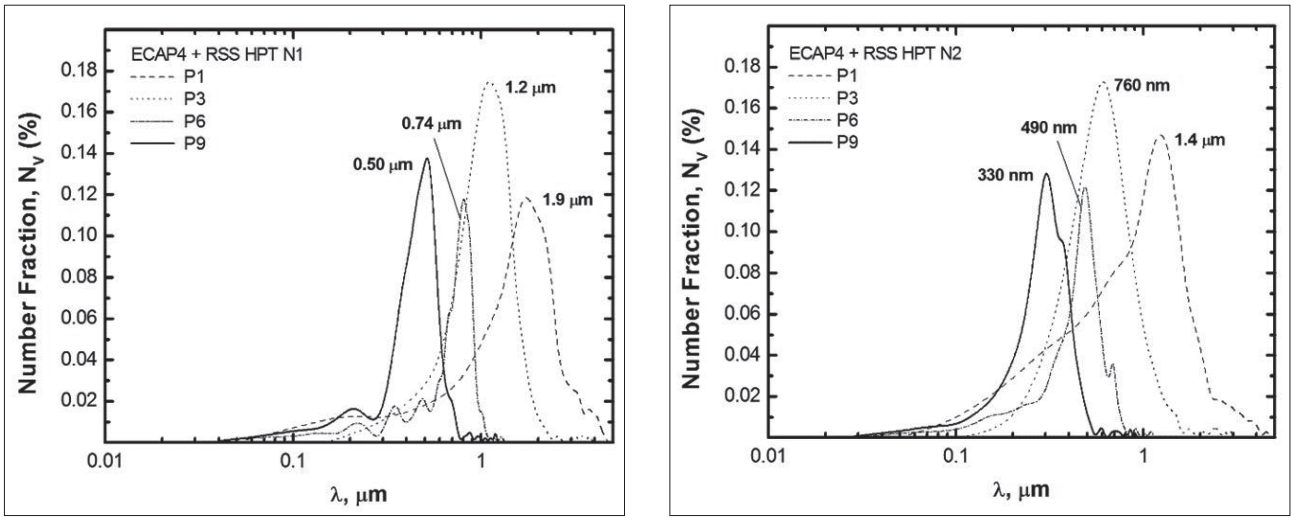

c) d)

Fig. 6 - Cell spacing evolution with ECAP-B_C/4 + CSS HPT and N = 1 revolution, P = 1-to-9 GPa, a); ECAP-B_C/4 + CSS HPT and N = 2 revolution, P = 1-to-9 GPa, b); ECAP-B_C/4 + RSS HPT and N = 1 revolution, P = 1-to-9 GPa, c); ECAP-B_C/4 + RSS HPT and N = 2 revolution, P = 1-to-9 GPa, d). Mean grain size is reported in the graph next to the corresponding distribution.
Evoluzione dimensionale della spaziatura delle celle, dopo ECAP-B_C/4 + CSS HPT e N = 1, P = 1-9 GPa, a); ECAP-B_C/4 + CSS HPT e N = 2, P = 1-9 GPa, b); ECAP-B_C/4 + RSS HPT e N = 1, P = 1-9 GPa, c); ECAP-B_C/4 + RSS HPT e N = 2, P = 1-9 GPa, d). I valori medi sono riportati in corrispondenza delle curve di distribuzione.

As for the nanoindentation hardness results, Fig. 7 shows the average values of the measurements taken across two mutually perpendicular diameters of the billet section (plane Z) after 1 ECAP and 4 ECAP-B_C passes. Due to a data accuracy of 2%, the experimental error corresponds to the data point in this and all the following nano-indentation hardness plots. It appears that the hardness increased from the edge to the central region in both cases. The hardness values from the edge to the center varied from 1.1 to 1.3 GPa, respectively, and went from 1.4 to 1.6 GPa, respectively, in ECAP-B_C/4. This means that the mean difference from the edge to the center is the same with increasing shear deformation, the only difference being the overall hardness rise with shear strain from 1 to 4 passes.

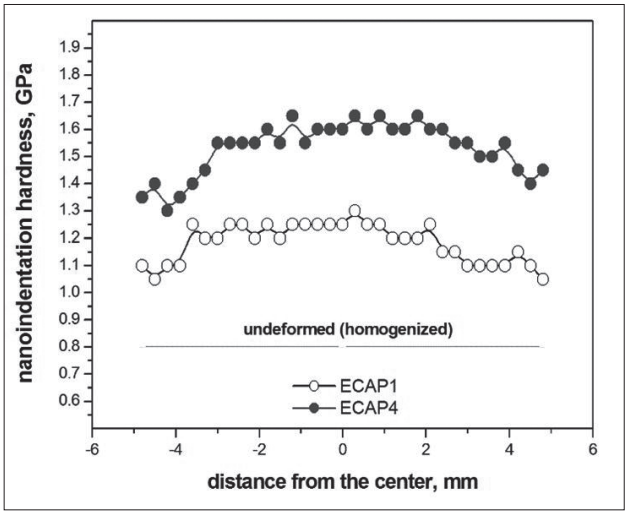

Fig. 7 - Nanoindentation hardness of ECAP/1 and ECAP-B_C/4.
The hardness of undeformed homogenized nickel is also reported as a solid horizontal line for comparison.
Durezza, misurata mediante nanoindentazione, dopo ECAP/1 e ECAP-B_C/4.
La durezza relativa alla condizione iniziale non deformata ed omogeneizzata è riportata nel grafico.

The hardness of the material after ECAP/1 + HPT (Fig. 8) steadily increased with HPT deformation strain, both in terms of pressure and number of revolutions. In this case, the differences in the values between the edge and the central regions accounted for lower hardness in the center than in the edge. It interesting to note that the edge-to-center hardness differences tend to vanish

as the applied HPT pressure increases. This trend of hardness homogenization tended to be faster as the number of revolutions increased (i.e., from 1 to 2).
All the findings reported in the case of the combined deformation ECAP/1 + HPT essentially holds also for the more severe deformation condition of ECAP-B_C/4 + HPT. Data obtained for the ECAP-B_C/4 + HPT were plotted as a function of shear strain and are reported in Fig. 9. In this case, the hardness differences between the edge and the central region are markedly larger when low HPT pressures are applied (namely, for P = 1, and 3 GPa, when using CSS HPT mode, and just for P = 1 GPa, when using RSS HPT mode). This hardness inhomogeneity fully vanished at P = 9 GPa, whatsoever the number of revolutions for the CSS HPT mode, and vanished at P = 9 GPa, only for N = 2 for the RSS HPT mode. The tendency to homogeneity seemed to be more effective when CSS was used (which reached P = 9 GPa, N =1, and P = 6 GPa, N = 2) compared to when RSS was used (where saturation was virtually reached only at P = 9 GPa, N = 2). Moreover, also the maximum hardness values that could be reached by the CSS HPT mode were higher compared to the RSS ones (H = 3.9 GPa, against H = 3.65 GPa).

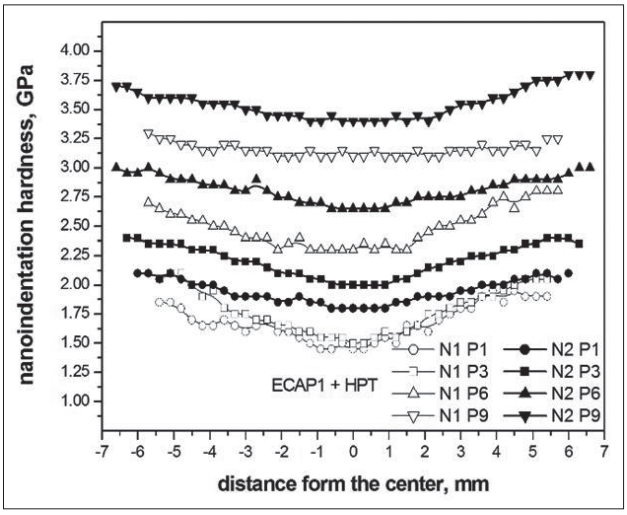

Fig. 8 - Nanoindentation hardness of ECAP/1 + HPT.
Durezza dopo ECAP/1 + HPT.

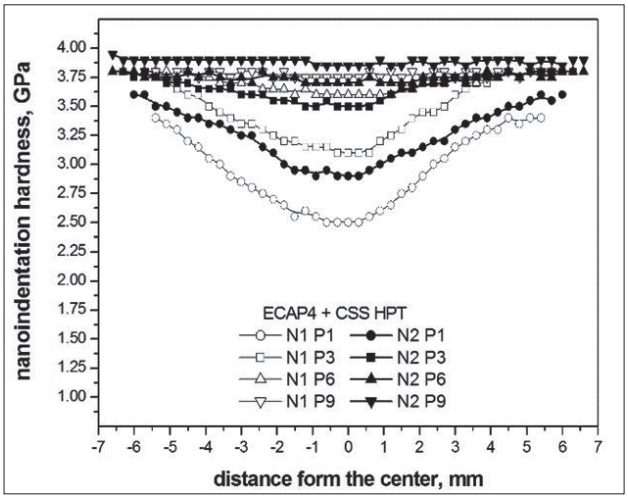

a)

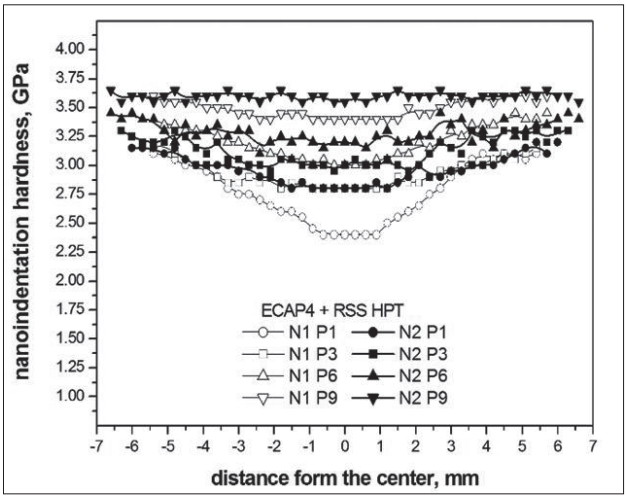

b)

Fig. 9 - Nanoindentation hardness of ECAP-B_C/4 + CSS HPT, a); ECAP-B_C/4 + RSS HPT, b).
Durezza dopo ECAP-B_C/4 + CSS HPT, a); ECAP-B_C/4 + RSS HPT, b).

DISCUSSION

In the present study, the observed microstructure grain refinement and size tendency to equiaxiality with cumulative shear strain by ECAP is fully consistent with other previous findings [30-37]. The microstructure evolution induced by the combined effect of ECAP and HPT was reported to lead to a greater amount of grain refinement with a rate that was significantly greater than that obtained by just using ECAP cumulative shear deformation. This microstructure aspect is largely in line with previously reported inspections [38-50] on both Ni and other metallic materials, such as steels [48] and titanium [41]. Several authors have reported that the stress inhomogeneities is inherent to the HPT deformation process [35,51-53]. Many others have reported on stress homogeneity and on saturation limit of microstructure refinement possibly achievable by HPT and, in some cases, this stress homogeneity has been reported to be a result of the combination of ECAP + HPT [13,34-50]. As in the present case, other authors have also reported on a microstructure refinement process which is highly promoted by the combined effect of ECAP and HPT compared to the ECAP or HPT single process ([13,43,44,54], to cite but few). In particular, Zhilyaev et al. [13] reported a significant decrease in the fraction of low-angle boundaries (i.e., sub-grains) in favour of the high-angle boundaries (i.e., grains) as the shear deformation cumulate in the order of ECAP, HPT, and ECAP + HPT. Similarly, even if only in the case of ECAP deformation, same dislocation boundary character promotion from low- to high-angle has been widely documented and reported by this author in several previous publications ([30,31], to cite but few).
Anyhow, this is the first time that the role of the plastic

deformation sense between ECAP and HPT is studied. Indeed, the both the microstructure cell, and related hardness saturation limits are strongly related to the way the deformation between ECAP and HPT proceeds. As a matter of fact, it was here showed that, whenever the deformation keep following the same path, between ECAP and HPT, the refining process limits and the hardness increment trends go fast and, therefore, are more effective. In a sake of a more exhaustive description of this interesting aspect, the observed grain size saturation limit can be correlated to the mechanical saturation of the measured nanoindentation hardness. The data reported in the Experimental Results section can thus be plotted as shown in Fig. 10. Here, the mean hardness of the edge and central regions at ECAP/4-B_C + HPT are plotted separately as a function of the HPT pressure.
It clearly appears that the hardness rate increases considerably faster when the CSS deformation mode is used instead of the RSS one. In particular, in the edge region of ECAP/4-B_C + CSS HPT, irrespective of the revolution regimes (i.e., for N = 1 and 2 revolutions), hardness increased very rapidly already for P = 1 and P = 3 GPa, to start to saturate for larger pressure levels. Similarly, the increase in hardness was particularly fast for P < 6 GPa in the central region of the same ECAP + HPT deformation mode, but here, a saturation limit was not reached at the maximum HPT pressure P = 9 GPa.

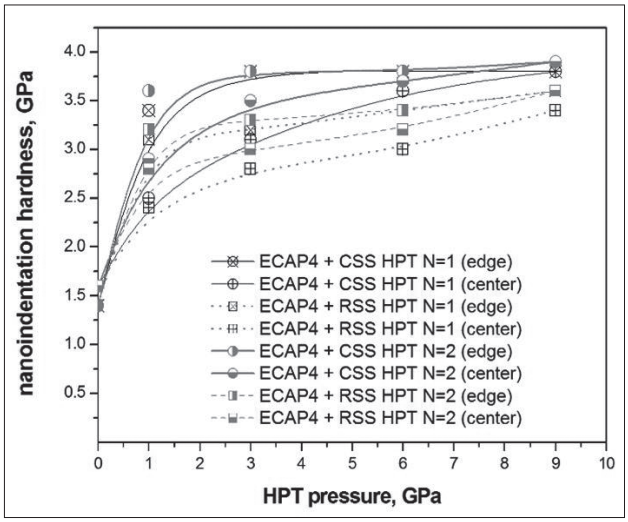

Fig. 10 - Mean hardness at the edge and central regions of the disks vs. HPT pressure for ECAP-B_C/4 + HPT.
Valori di durezza media in corrispondenza della periferia e delle zone centrali dei dischetti in funzione della pressione imposta durante HPT, per ECAP-B_C/4 + HPT.

The hardness increment, with HPT pressure, was significant, but remarkably lower, in the case of ECAP/4-B_C + RSS HPT, both inthe edge and central regions and for N = 1, and 2 anvil revolutions. Moreover, in the latter ECAP + HPT deformation mode, no hardness saturation was reached.
The different hardness evolution, between CSS and RSS mode, can be attributed to a faster promotion of the low-angle boundaries to high-angle boundaries, during shear deformation when shear direction and sense, followed by ECAP and the following HPT, were the same. That is, when the sense of shear deformation between ECAP and HPT is cooperative, the rate of generation of the high-angle boundaries, either from the already existing low-angle boundaries, and from the newly formed boundaries, is higher than in the case of opposite shear sense of deformation between ECAP and HPT. This argumentation is supported by a previously published study by this author [30]. The study showed a direct correlation between the cumulative shear deformation during ECAP and the progressive evolution and generation of high-angle boundaries at the expense of the low-angle boundaries.
It is interesting to note that the mean values in the edge region at N = 1 revolution collimate to the values obtained at N = 2 revolutions, irrespective of the specific ECAP + HPT deformation mode that was followed (i.e., this holds for CSS and RSS modes). Remarkably, the hardness values at both the edge and center of the disk, at HPT P = 9 GPa, and N = 1 and 2 revolutions, essentially collimated to a common value of H = 3.8 – 3.9 GPa. This, indeed, is another interesting aspect of the combination of ECAP + HPT deformations. That is, when only HPT is used to refine the microstructure of a metallic alloy, the refining process in the periphery of the disc, and thus the corresponding hardness increment, is always slower that in the central regions of the HPT disc. It wash here shown, that by combining the ECAP + HPT, and using the same sense of plastic deformation, the hardness tends to homogenise throughout the extension of the HT disc, i.e., form the periphery to the center.
By averaging the hardness data along the entire extension of the disk diameter, that is, from the edge to the center (Fig. 11), the saturation limit appeared to be more evident. Fig. 11 clearly shows that hardness saturates at H = 3.8 GPa already at P = 3 GPa after 2 revolutions by using the CSS HTP deformation mode. When the revolution is halved to 1, the saturation limit is delayed, and it only reaches for P 9 GPa. In the case of the RSS HPT deformation mode, the hardness did not seem to reach a saturation limit within the shear deformation exerted by the HPT (that is up to the maximum strain of P = 9 GPa, N = 2 revolutions: $\varepsilon_{true}^{ECAP+HPT} = 9.5$).

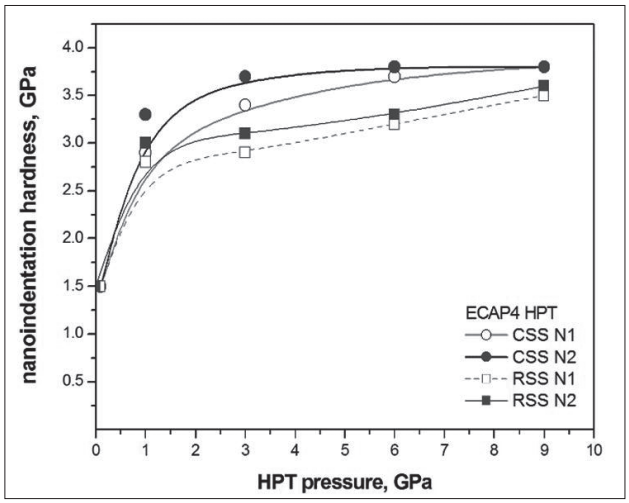

Fig. 11 - Mean hardness along the diameter of the disk vs. HPT pressure for ECAP-B_C/4 + HPT.
Valori di durezza media lungo il diametro dei dischetti in funzione della pressione imposta durante HPT, per ECAP-B_C/4 + HPT.

In other studies, it seemed that a saturation limit from 3.8 - 4 GPa could be reached in this latter shear deformation configuration (RSS) but for larger deformation levels than those used in the present study. The saturation of the refined cell structure and hardness reported here, agree, to some extent, with the results reported by Zhilyaev et al. [39]. They reported that in high purity Ni, subjected to HPT at 5 complete revolutions for pressures ranging 1-to-9 GPa, the differences in the hardness between the edge and central region steadily tended to collimate to a common value with the applied pressure. Their results also seem to suggest that a saturation limit of ~3.6 – 4 GPa could be reached. Similar conclusions can be driven in the case of the data reported by Korznikova et al. [38] where the number of HPT revolutions ranged from 0.1-to-5, and the deformation pressure was P = 4 GPa. In both cases, the hardness was measured by conventional methods, i.e., by micro-hardness tests, and thence the accuracy of data has to be considered higher in the present case where a much more accurate and "localized" method of measurement (nanoindentation) was adopted.

The reported hardness results agree quite well with the observed microstructure evolution under ECAP + HPT. In fact, Fig. 6 reports a saturation limit of reduction of cell spacing of ~0.3 μm, at P = 3 GPa, and P = 6 GPa, for N = 1, and 2 revolutions, respectively, when the CSS HPT mode was used. These deformation levels, at which the grain size saturation occurred, are the ones for which a saturation limit of hardness at 3.8 GPa was reached. This ultimately implies that the microstructure refining process directly drives the hardness rise, and whenever the microstructure refining process reaches a physical limit, i.e., saturates, the hardness stops increasing, and thus saturates accordingly. Yet, present findings clearly indicate the importance of specify the shear direction and sense of deformation followed by ECAP and HPT, as it consistently influence the microstructure and hardness evolution. To the author's knowledge, this process issue and its role on the microstructure and hardness evolution, is here recognized for the first time.

In order to exploit the possibility to rationalize the observed hardness saturation with cumulative shear strain so as to better correlate it to the microstructure cell and grain refinement saturation process, data were plotted in Fig. 12 in terms of the total equivalent shear strain, $\varepsilon_{true}^{ECAP+HPT} = \varepsilon_{true}^{ECAP} + \varepsilon_{true}^{HPT}$.

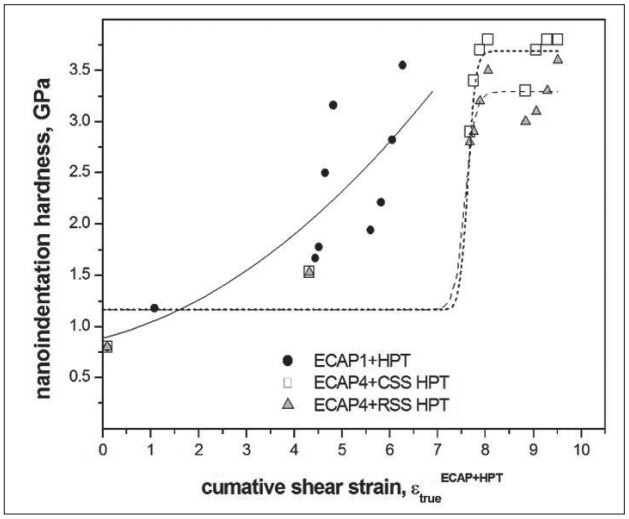

Fig. 12 - Mean hardness along the diameter of the disk vs. cumulative strain, $\varepsilon_{true}^{ECAP+HPT}$, for all shear deformation levels: ECAP and ECAP + HPT. Interpolation curves are plotted, and sigmoidale-like curves was be used to describe the saturation behavior of the ECAP-B_C/4 + HPT conditions.

Valori di durezza media lungo il diametro in funzione della deformazione plastica di taglio imposta mediante ECAP + HPT, $\varepsilon_{true}^{ECAP+HPT}$. I dati sperimentali sono stati interpolati mediante curve di interpolazione sigmoidali.

In the plot of Fig. 12, a sigmoidale-like interpolation curve was applied to the experimental data for the ECAP-B_C/4 + CSS HPT deformation mode and for the ECAP-B_C/4 + RSS HPT deformation mode. The interpolating curve for ECAP/1 + HPT cannot be described using a sigmoidale-like curve as it appeared not to reach a saturation limit. The plots in Fig. 12 clearly show that hardness saturation occurs at a total strain $\varepsilon_{true}^{ECAP+HPT} = 8$, for ECAP-$B_C$/4 + HPT with whatsoever rotation sense between ECAP and HPT was used. On the other hand, the maximum hardness saturation level reached by following the CSS deformation mode in HPT (i.e., a co-operating shear deformation between ECAP route B_C and HPT, by rotating the plane Z, as defined in ECAP, to the same rotation sense between ECAP and HPT) was higher by around 10% with respect to what was obtained by following the RSS deformation mode (i.e., a reversing shear deformation between ECAP route B_C and HPT). As a matter of fact, the reported data seem to suggest that, by further accumulating deformation by RSS mode (i.e., for $\varepsilon_{true}^{ECAP+HPT} > 9.5$), same saturation hardness levels as those already reached at $\varepsilon_{true}^{ECAP+HPT} = 8$ by the CSS mode would possibly be reached. In other words, the CSS HPT mode appeared to be more effective compared to the RSS one in hardening and, ultimately, in refining the microstructure of pure nickel. The plotted data referring to ECAP/1 + HPT appear to be much more scattered compared to those observed for ECAP-B_C/4 + HPT, and in fact a saturation limit was not reached. The far less data scattering in ECAP-B_C/4 + HPT is believed to be due to the fully dislocation reorganization from tangled and low-angle boundaries, to cell (subgrain) and grain boundaries, respectively. This dislocation boundary misorientation evolution is driven by a 360° sample rotation around its symmetry axis after the full

rotational shear deformation cycle occurred by ECAP via route B_C. This microstructural aspect and mechanical implications have been discussed in a previously published work by this author [30].

CONCLUSIONS

The present study examined the development of grain structure and evolution of hardness during a combined severe plastic deformation processing using equal-channel angular pressing (ECAP) followed by high-pressure torsion (HPT) of pure nickel. For the first time here, two different ways of deformation by HPT with respect to ECAP route B_C were considered; one with the same sense of rotation between ECAP and HPT and another one with reverse sense of rotation.

The combined action of ECAP and HPT led to the formation of a reasonably uniform cell structure with a cell diameter down to ~ 280 nm. This size value was obtained at the maximum strain levels ($\varepsilon_{true}^{ECAP+HPT} > 8$).

A saturation limit of cell size refinement of ~ 280 nm was reached only when the same sense of rotation between HPT and ECAP was used. This was reached at ECAP-B_C/4 (counter clockwise rotation) + HPT for P = 6 GPa and N = 1 counter clockwise revolution, and it was anticipated to P = 3 GPa as the number of revolutions doubled.

No microstructure saturation limit was observed when the sense of rotation between ECAP-B_C and HPT was opposite.

Hardness measurements were carried out using nanoindentation in order to have a highly localized set of measurements. It was found that hardness saturated at P > 8 GPa in ECAP-B_C/4 + HPT using both senses of HPT rotation compared to ECAP. The only difference concerned the saturation level which was higher by 10 % in the case of co-operating shear strain (with the same sense of rotation) between ECAP and HPT. A saturation limit with values same as the ones reached using the co-operating shear strain deformation is likely to be obtained at larger deformation levels in the case of the HPT reversing shear deformation mode.

A homogenization of the HPT disc (from edge to center) was obtained at the maximum deformation levels, that is for $\varepsilon_{true}^{ECAP+HPT} > 8$. This homogenization tendency was more effective by using a concurrent sense of shear deformation between ECAP and HPT, that is whenever the shear deformation follows the same direction.

The experimental results provide a very clear demonstration of the advantage of processing materials through a combination of ECAP followed by HPT, both in terms of microstructure refinement, and metal hardening efficiency. The role of the shear deformation direction and accumulation, between ECAP and HPT, was recognized and outlined for the first time here. It was found that the cooperative shear direction between ECAP + HPT, led to a faster saturation of hardness and microstructure refinement, compared to a reversing shear direction.

REFERENCES

[1] K. NEISHI, Z. HORITA, T.G. LANGDON. Grain refinement of pure nickel using equal-channel angular pressing. Mater. Sci. Eng. A325, 2002, 54-8.

[2] L.E. MURR. Temperature coefficient of twin-boundary energy: The determination of stacking-fault energy from the coherent twin-boundary energy in pure F.C.C. metals. Scripta Metall. 6, 1972, 203-8.

[3] L.S. TOTH, C. GU. Ultrafine-grain metals by severe plastic deformation Materials Characterization. Mater. Charact. 92, 2014, 1-14.

[4] R.Z. VALIEV, T.G. LANGDON. Principles of equal-channel angular pressing as a processing tool for grain refinement. Prog. Mater. Sci. 51, 2006, 881-981.

[5] M. FURUKAWA, Z. HORITA, M. NEMOTO, R.Z. VALIEV, T.G. LANGDON. Acta Mater. 44, 1996, 4619-29.

[6] M. KAMACHI, M. FURUKAWA, Z. HORITA, T.G. LANGDON. A model investigation of the shearing characteristics in equal-channel angular pressing. Mater. Sci. Eng. A347, 2003, 223-30.

[7] M. FURUKAWA, Z. HORITA, T.G. LANGDON. Factors influencing the shearing patterns in equal-channel angular pressing. Mater. Sci. Eng. A332, 2002, 97-109.

[8] V.M. SEGAL, V.I. REZNIKOV, A.E. DROBYSHEVSKIY, V.I. KOPYLOV. Plastic working of metals by simple shear. Russ. Metall. 1, 1981, 99-105.

[9] R.Z. VALIEV, N.A. KRASILNIKOV, N.K. TSENEV. Plastic deformation of alloys with submicron-grained structure. Mater. Sci. Eng. A137, 1991, 35-40.

[10] A. REBHI, T. MAKHLOUF, N. NJAH, Y. CHAMPION, J.-P. COUZINIE'. Characterization of aluminum processed by equal channel angular extrusion: Effect of processing route. Mater.Charact. 60, 2009, 1489-95.

[11] T.C. LOWE, R.Z. VALIEV. Producing nanoscale microstructures through severe plastic deformation. JOM-J. Minerals Metals Mater. Soc. 52, 2000, 27-8.

[12] A.P. ZHILYAEV, B.M. KIM, G.V. NURISLAMOVA, M.D. BARO', J.A. SZPUNAR, T.G. LANGDON. Orientation imaging microscopy of ultrafine-grained nickel. Scripta Mater. 46, 2002, 575-80.

[13] A.P. ZHILYAEV, B.K. KIM, J.A. SZPUNAR, M.D. BARO', T.G. LANGDON. The microstructural characteristics of ultrafine-grained nickel. Mater. Sci. Eng. A391, 2005, 377-89.

[14] J. WONGSA-NGAM, M. KAWASAKI, T.G. LANGDON. A comparison of microstructures and mechanical properties in a Cu-Zr alloy processed using different SPD techniques. J. Mater. Sci. 48, 2013, 4653-60.

[15] V.V STOLYAROV, Y.T. ZHU, T.C. LOWE, R.K. ISLAMAGALIEV, R.Z. VALIEV. A two step SPD processing of ultrafine-grained titanium.N anostruct. Mater. 11, 1999, 947-54.

[16] A.P. ZHILYAEV, A.A. GIMAZOV, E.P. SOSHNIKOVA, Á. REVESZ, T.G. LANGDON. Microstructural characteristics of nickel processed to ultrahigh strains by high-pressure torsion. Mater. Sci. Eng. A489, 2008, 207-12.

[17] J. WONGSA-NGAM, H. WEN, T.G. LANGDON. Microstructural evolution in a Cu-Zr alloy processed by a combination of ECAP and HPT. Mater. Sci. Eng. A579, 2013, 126-35.

[18] V.V POPOV, E.N. POPOVA, A.V. STOLBOVSKIY. Nanostructuring Nb by various techniques of severe plastic deformation. Mater. Sci. Eng. A539, 2012, 22-9.

[19] E.N. POPOVA, V.V. POPOV, E.P. ROMANOV, V.P. PILYUGIN. Thermal Stability of Nanocrystalline Nb produced by Severe plastic deformation. Phys. Metals Metall. 101, 2006, 52-7.

[20] E.N. POPOVA, V.V. POPOV, E.P. ROMANOV, V.P. PILYUGIN. Effect of the degree of deformation on the structure and thermal stability of nanocrystalline niobium produced by high-pressure torsion. Phys. Metals Metall. 103, 2007, 407-13.

[21] K. NAKASHIMA, Z. HORITA, M. NEMOTO, T.G. LANGDON. Development of a multi-pass facility for equal-channel

angular pressing to high total strains. Mater. Sci. Eng. A281, 2000, 82-7.
[22] Y. IWAHASHI, J. WANG, Z. HORITA, M. NEMOTO, T.G. LANGDON. Principle of equal-channel angular pressing for the processing of ultra-fine grained materials. Scripta Mater. 35, 1996, 143-6.
[23] M.V. DEGTYAEREV, T.I. CHASHCHUKHINA, L.M. VORONOVA, L.S. DAVYDOVA, V.P.PILYGIN. Deformation strengthening and structure of structural steel upon shear under pressure. Phys Metal. Metall. 90, 2000, 604-11.
[24] B.M. EFROS, V.P. PILYGIN, A.M. PATSELOV, Y.Y. BEYGELZIMAR, N. EFROS. In: Zhu YT, Langdon TG, Mishra RS, Semiatin SL, Saran MJ, Lowe TC, editors. Ultrafine grained materials II. Warrendale, PA: The Minerals, Metals and Materials Society; 2002, p. 193-8.
[25] G.M. PHARR. Measurement of mechanical properties by ultra-low load indentation. Mater. Sci. Eng. A253, 1998, 151-9.
[26] M. CABIBBO, P. RICCI, R. CECCHINI, Z. RYMUZA, J. SULLIVAN, S. DUB, S. COHEN. An international round-robin calibration protocol for nanoindentation measurements. Micron 43, 2012, 215-22.
[27] NANOINDENT FP7 project: NMP3-CA-2008-218659: "Creating and disseminating novel nanomechanical characterisation techniques and standards", web-site: http://www.nanoindent.eu
[28] M.F. DOERNER, W.D. NIX. A method for interpreting the data from depth-sensing indentation instruments. J. Mater. Res. 1, 1986, 601-9.
[29] F.J. HUMPHREYS. Quantitative metallography by electron backscattered diffraction. J. Microscopy 195, 1999, 170-85.
[30] M. CABIBBO, W. BLUM, E. EVANGELISTA, M.E. KASSNER, M. MEYERS. Transmission Electron Microscopy Study of Strain-Induced Low- and High-Angle Boundary Development in Equal-Channel Angular-Pressed Commercially Pure Aluminum. Metall. Mater. Trans. 39A, 2008, 181-9.
[31] M. Cabibbo. Microstructure strengthening mechanisms in different equal channel angular pressed aluminum alloys. Mater. Sci. Eng. A560, 2013, 413-32.
[32] A. VEVECKAS, M. CABIBBO, T.G. LANGDON. A characterization of microstructure and microhardness on longitudinal planes of an Al-Mg-Si alloy processed by ECAP. Mater. Charact. 84, 2013, 126-33.
[33] M. KAWASAKI, Z. HORITA, T.G. LANGDON. Microstructural evolution in high purity aluminum processed by ECAP. Mater.Sci. Eng. A524, 2009, 143-50.
[34] J. GUBICZA, N.Q. CHINH, J.L. LABAR, S. DOBATKIN, Z. HEGEDUS, T.G. LANGDON. Correlation between microstructure and mechanical properties of severely deformed metals. J. All. Comp.d 483, 2009, 271-4.
[35] H.W. ZHANG, X. HUANG, N. HANSEN. Evolution of microstructural parameters and flow stresses toward limits in nickel deformed to ultra-high strains. Acta Mater. 56, 2008, 5451-65.
[36] H.W. ZHANG, X. HUANG, R. PIPPAN, N. HANSEN. Thermal behavior of Ni (99.967% and 99.5% purity) deformed to an ultra-high strain by high pressure torsion. Acta Mater. 58, 2010, 1698-707.
[37] K.S. RAJU, M.G. KRISHNA, K.A. PADMANABHAN, K. MURALEEDHARAN, N.P. GURAO, G. WILDE. Grain size and grain boundary character distribution in ultra-fine grained (ECAP) nickel. Mater. Sci. Eng. A491, 2008, 1-7.
[38] F. KHODABAKHSHI, M. HAGHSHENAS, H. ESKANDARI, B. KOHBOR. Hardness–strength relationships in fine and ultra-fine grained metals processed through constrained groove pressing. Mater. Sci. Eng. A636, 2015, 331-9.
[39] A.P. ZHILYAEV, S. LEE, G.V. NURISLAMOVA, R.Z. VALIEV, T.G. LANGDON. Microhardness and microstructural evolution in pure nickel during high-pressure torsion. Scripta Mater. 44, 2012, 2753-8.
[40] R.Z. VALIEV, Y.V. IVANISENKO, E.F. RAUCH, B. BAUDELET. Structure and deformation behaviour of Armco iron subjected to severe plastic deformation. Acta Mater. 44, 1996, 4705-12.
[41] M. FURUKAWA, Z. HORITA, M. NEMOTO, R.Z. VALIEV, T.G. LANGDON. Factors Influencing the Flow and Hardness of Materials with Ultrafine Grain Sizes. Phil. Mag. A78, 1998, 203-15.
[42] J. PHILIBERT. Atom Movement, Diffusion and Mass Transportation in Solids, Editions de Physique, Les Ulis, France 421-520, 1991, 110-11.
[43] A.P. ZHILYAEV, J. GUBICZA, G. NURISLAMOVA, A. REVESZ, S. SURINACH, M.D. BARO', T. UNGAR. Microstructural characterization of ultrafine-grained nickel. Phys. Stat. Sol. A 198, 2003, 263-71.
[44] S.D. TERHUNE, D.L. SWISHER, K. OH-ISHI, Z. HORITA, T.G. LANGDON, T.R. McNELLEY. An Investigation of Microstructure and Grain-Boundary Evolution During Eca Pressing of Pure Aluminum. Metall. Mater. Trans. 33A, 2002, 2173-84.
[45] A.P. ZHILYAEV, G.V. NURISLAMOVA, B.K. KIM, M.D. BARO', J.A. SZPUNAR, T.G. LANGDON. Acta Mater. 51, 2003, 753-65.
[46] G. SAKAI, Z. HORITA, T.G. LANGDON. Grain refinement and superplasticity in an aluminum alloy processed by high-pressure torsion. Mater. Sci. Eng. A393, 2005, 344-51.
[47] Z. HORITA, T.G. LANGDON. Microstructures and microhardness of an aluminum alloy and pure copper after processing by high-pressure torsion. Mater. Sci. Eng. A410-411, 2005, 422-5.
[48] A.P. ZHILYAEV, S. LEE, G.V. NURISLAMOVA, R.Z. VALIEV, T.G. LANGDON. Microhardness and microstructural evolution in pure nickel during high-pressure torsion. Scripta Mater, 44, 2001, 2753-8.
[49] A.P. ZHILYAEV, K. OH-ISHI, T.G. LANGDON, T.R. McNELLEY. Microstructural evolution in commercial purity aluminum during high-pressure torsion. Mater. Sci. Eng. A410-411, 2005, 277-80.
[50] C. XU, Z. HORITA, T.G. LANGDON. The Evolution of Homogeneity in Processing by High-Pressure Torsion. Acta Mater. 55, 2007, 203-12.
[51] R. VORHAUER, R. PIPPAN. On the homogeneity of deformation by high pressure torsion. Scripta Mater. 51, 2004, 921-5.
[52] H. JIANG, Y.T. ZHU, D.B. BUTT, I.V. ALEXANDROV, T.C. LOWE. Microstructural evolution, microhardness and thermal stability of HPT-processed Cu. Mater. Sci. Eng. A290, 2000, 128-38.
[53] Z. YANG, U. WELZEL. Microstructure-microhardness relation of nanostructured Ni produced by high-pressure torsion. Mater. Lett. 59, 2005, 3406-9.
[54] Y.R.KOLOBOV, N.V. GIRSOVA, K.V. IVANOV, G.P. GRABOVETSKAYA, O.B. PEREVALOVA. The Structural Features and Mechanical Properties of Submicrocrystalline Nickel Produced by Severe Plastic Deformation. Russian Phys. J. 45, 2002, 547-52.